IMAV2017-27
http://www.imavs.org/pdf/imav.2017.27

Collision Avoidance of multiple MAVs using a multiple Outputs to Input Saturation Technique

C. Chauffaut, L. Burlion*, F. Defaÿ and H. de Plinval
ISAE-Research, Toulouse, France
ONERA - The French Aerospace Lab, Toulouse, France

ABSTRACT

This paper proposes a novel collision avoidance scheme for MAVs. This scheme is based on the use of a recent technique which is based on the transformation of state constraints into time-varying control input saturations. Here, this technique is extended so as to ensure collision avoidance of a formation of up to three MAVs. Experimental results involving three A.R drones show the efficiency of the approach.

1 INTRODUCTION

The Unmanned Aicraft Integration into civil Airspace is a major challenge which involves considering new uses for these vehicles while reducing technical barriers related to safety. Underlying many of the safety challenges is the issue of assessing the capability of one operator to simultaneously control multiple vehicles. The need for basic formation keeping techniques and especially collision avoidance capability is surely the most critical in order to enable one operator to focus on the supervision of the fleet of Unmanned Aerial Vehicles (MAVs).

A large research effort has been focused on the synchronization and formation control of a fleet of MAVs (see e.g the survey paper [1] and the references therein). Many interesting problems have been adressed so far : to cite a few, researchers have considered formation control problems dealing with leader-follower approaches [2, 3, 4, 5], cooperative sensing [6, 7] or communication delays [8]. Another difficult problem is the collision avoidance between members of a fleet and/or the environment. This problem was mainly adressed using the well known potential field method [9, 10] which is not straightforward to apply when one considers underactuated MAVs (as discussed in the open problems section 8.3 of [11]) or when one would like to choose a sophisticated dynamical guidance laws when the MAVs are far from each other.

This paper introduces a novel anti-collision technique, different from the potential field methods : it makes use of the Output to Input Saturation Transformation (OIST) method. First presented in [12], and later applied to visual servoing [13, 14] and load alleviation for a civil aircraft [15]. The principle of this method is to transform a desired bound on a variable of interest into a saturation expressed on the control inputs. One of the main features of this approach is that a smooth switch between a nominal (local) control law and a saturated (global) one can be performed. Also, once transformed into a saturated input control problem, the formulation boils down to a well-known problem for which an abundant literature is available. Thus, the anti-windup framework [16] can be applied to the problem transformed via OIST [17]. In this paper, we present experimental results which demonstrate the successful application of this methodology to a triangular formation of MAVs.

Section 1 indroduces the problematic of obstacle avoidance and formation flying. Section 2 presents the simplified dynamic model used for the control. In Section 3, the theoretical development used to ensure safe collision avoidance based on the OIST framework is presented. Then Section 4 describes the system architecture. Section 5 describes the experimental results. Finally, conclusions follow.

2 MAV DYNAMIC MODEL FOR CONTROL

For the control synthesis, the MAV is modeled as a 3 DOF mass without taking the drag of the mav into account. The considered control input is the thrust vector. This thrust can easily be converted into a global thrust provided by the rotors velocities, and its orientation which may be obtained by differences between these velocities. As a result, from now on, we consider that the thrust vector may be chosen as if it were the control input. The equation of the dynamics is given as:

$$m\ddot{\boldsymbol{\xi}} + \begin{pmatrix} 0 \\ 0 \\ mg \end{pmatrix} = \mathbf{F_d} \tag{1}$$

where $\boldsymbol{\xi} := [x\ ,\ y\ ,\ z]^T \in \mathbb{R}^3$ is the MAV position and where $\mathbf{F_d} := [F_{d,x}\ ,\ F_{d,y}\ ,\ F_{d,z}]^T \in \mathbb{R}^3$ is the control input.

2.1 Inner loop controller (PX4)

The experiments will be based on the framework presented in Section 4 which is done by two separate cards and control dynamics. Figure 1 describes the data flow between cards and MAV.

The attitude control inner loop is made by the pixhawk communauty, only the tunning of the gain have been tuned in the lab. Using the offboard mode, the baseline postion control combined to the OIST methodology send directly the

*Corresponding author: laurent.burlion(at)onera.fr

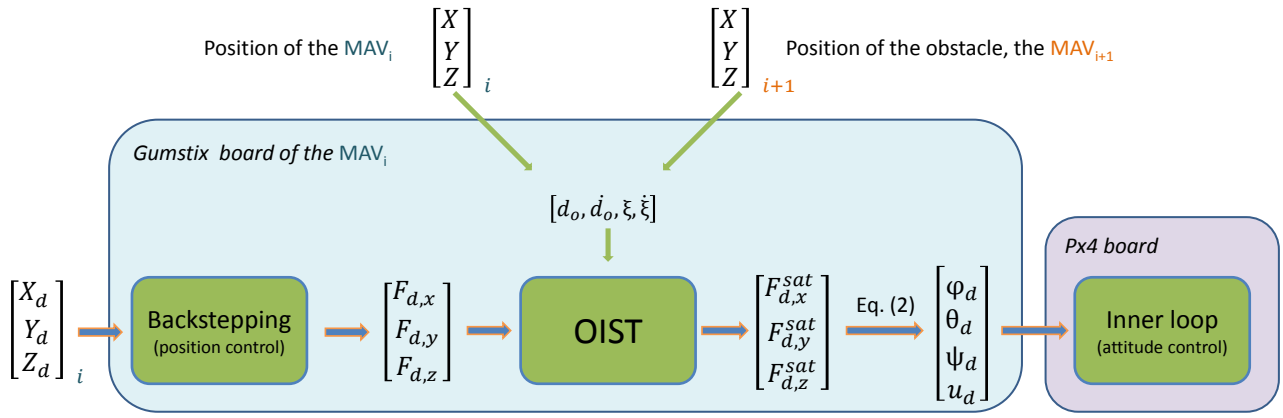

Figure 1: Output to Input Saturation Transformation methodology diagram

Attitude Target $(\varphi_d, \theta_d, \psi_d, u_d)$ at the PX4 board. Figure 2 presents the actual inner loop dynamics and response. One can see the presence of static errors, and the slowness of the dynamics. These phenomena may be explained by the lack of integral term in the attitude loop of the PX4, and also by the poor capabilities of the AR drone platform – especially with the weight added for our experiments. The nominal thrust command is arround 70 percent.

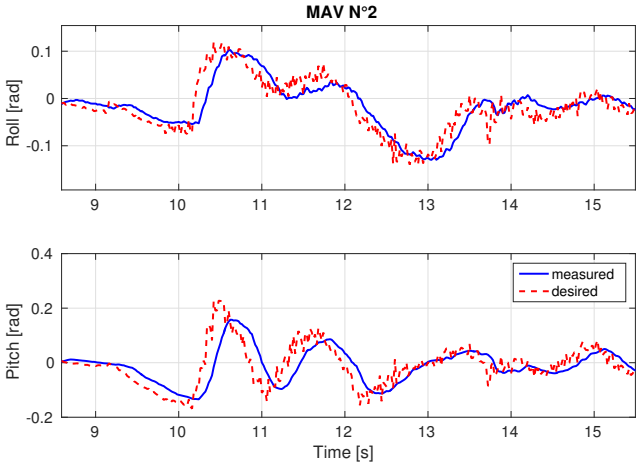

Figure 2: Attitude control dynamics

2.2 *Baseline controller (backstepping)*

The baseline controller $[F_{d,x}, F_{d,y}, F_{d,z}]$ used was developed at ISAE for trajectory tracking. More details on this control law can be found in [18].

The computed control input is expressed in terms of the thrust vector, as said earlier in this paper; it may be converted into the desired roll φ_d, pitch θ_d and thrust u_d through the simple following computations:

$$\begin{pmatrix} \varphi_d \\ \theta_d \\ u_d \end{pmatrix} = \begin{pmatrix} \text{atan2}(F_{d,y}, F_{d,z}) \\ \text{atan2}(-F_{d,x}, \sqrt{F^2_{d,y} + F^2_{d,z}}) \\ \sqrt{F^2_{d,x} + F^2_{d,y} + F^2_{d,z}} \end{pmatrix} \quad (2)$$

The desired roll φ_d, pitch θ_d and thrust u_d are then transmitted as reference for the inner loop. The desired yaw ψ_d will be equal to zero.

3 OUTPUT TO INPUT SATURATION TRANSFORM (OIST) MAV AVOIDANCE

The OIST methodology applies to the aforementioned baseline controller [18], which output is saturated through the method in order to force the variable of interest to abide by the predefined constraints

3.1 *Useful notations*

Given two real numbers $x_{\min} < x_{\max}$, we note:

$$x \longmapsto Sat^{x_{\max}}_{x_{\min}}(x) = \max\left(x_{\min}, \min(x, x_{\max})\right) \quad (3)$$

the saturation function of a variable x between $x_{\min}$ and $x_{\max}$.
With an abuse of notation:

$$Sat^{+\infty}_{x_{\min}}(x) = \max(x_{\min}, x) \quad (4)$$

3.2 *OIST methodology for a moving obstacle avoidance*

Here, we propose to revisit the OIST design of [14] which was used to make a MAV avoid some obstacles. In this preliminary work, the OIST methology was successfully used for obstacle avoidance but was "switched off" (by a simple logic detailed in the experiment section of the paper) on the frontier of the obstacles in order to avoid the MAV to be stuck on them. As we shall see, an additional output constraint is here used to circumvent this problem : roughly speaking, the OIST method is not only used to avoid another

MAV but also to avoid that a MAV is stuck on another one by imposing its (orthoradial) velocity not to vanish on it. We also slightly extend the OIST framework to take into account the fact that the obstacle (other MAV) can now move (in the same (x,y) plane as the MAV), which requires to measure the velocity and acceleration of the obstacle.

The following assumptions are necessary to apply this novel OIST technique.
At any time:

- the distance d_o between the MAV and the other MAV is measured.
- the obstacle is supposed to be included inside a circle which is centered on (x_o, y_o, z) and whose radius is always lower than $d_{o,inf}$ in the (x, y) plane The obstacle being possibly in motion, its velocity (resp. acceleration) vector $(\dot{x}_o, \dot{y}_o)$ (resp. $(\ddot{x}_o, \ddot{y}_o)$) are supposed to be measured in the (x, y) plane.
- the MAV desired position $\boldsymbol{\xi_d}$ is sufficiently far from the obstacle so that the mission is feasible.

Figure 1 represents the general principle of the OIST methodology when extended to the MAV avoidance problem.
Let us define the following quantities:

$$d_{o,2} := d_o^2 = (x - x_o)^2 + (y - y_o)^2 \tag{5}$$

and

$$\phi_\perp = -(y - y_o)v_x + (x - x_o)v_y \tag{6}$$

To avoid a collision, the following constraint must be satisfied:

$$d_{o,2} \geq d_{o,inf}^2 \tag{7}$$

Moreover, to avoid staying stuck on the obstacle boundary, we consider the following additional constraint:

$$\phi_\perp \geq d_{o,inf} v_\perp^\# - \kappa_3(d_{o,2} - d_{o,inf}^2) \tag{8}$$

where $v_\perp^\# > 0, \kappa_3 > 0$

Such an inequality simply expresses the constraint that the orthoradial velocity (component of the MAV velocity which is perpendicular to a line relating the MAV to the obstacle center) cannot be null on the obstacle boundary so that the MAV is forced to keep turning around the obstacle.

Remark 1 *another possibility is to use the constraint:*

$$\phi_\perp \leq -d_{o,inf} v_\perp^\# + \kappa_3(d_{o,2} - d_{o,inf}^2) \tag{9}$$

where $v_\perp^\# > 0, \kappa_3 > 0$. This would change the sign of $v_\perp$ on the obstacle. This other possiblity can be considered as another degree of freedom of the method which deserves to be studied in the future.

Following the OIST methodology (see e.g. the guidelines of [13], subsection II-D)), we compute the successive time derivatives of the constrained outputs $d_{o,2}$ and $\phi_\perp$ till the input terms appear. Deriving two times (resp. one time) $d_{o,2}$ (resp. $\phi_\perp$), we obtain:

$$\begin{cases} \ddot{d}_{o,2} = 2\Big((x - x_o)\left(\frac{F_{d,x}}{m} - \ddot{x}_o\right) + (y - y_o)\left(\frac{F_{d,y}}{m} - \ddot{y}_o\right) \\ \qquad +(\dot{x} - \dot{x}_o)^2 + (\dot{y} - \dot{y}_o)^2\Big) \\ \dot{\phi}_\perp = -(y - y_o)\frac{F_{d,x}}{m} + (x - x_o)\frac{F_{d,y}}{m} - (\dot{y} - \dot{y}_o)v_x \\ \qquad +(\dot{x} - \dot{x}_o)v_y \end{cases} \tag{10}$$

We now consider the following matrix:

$$\mathbf{M_o}(\boldsymbol{\xi}) := \frac{2}{m}\begin{bmatrix} x - x_o & y - y_o \\ -(y - y_o) & x - x_o \end{bmatrix} \tag{11}$$

which is invertible when $det(\mathbf{M_o}) = d_{o,2} \geq d_{o,inf}^2 > 0$.
Using $\mathbf{M_o}$, we rewrite (10) as follows:

$$\begin{bmatrix} \ddot{d}_{o,2} \\ 2\dot{\phi}_\perp \end{bmatrix} = \mathbf{M_o}(\boldsymbol{\xi})\begin{bmatrix} F_{d,x} \\ F_{d,y} \end{bmatrix} + \begin{bmatrix} D_1 \\ 2D_2 \end{bmatrix} \tag{12}$$

where

$$\begin{aligned} D_1 &= 2(\dot{x} - \dot{x}_o)^2 + 2(\dot{y} - \dot{y}_o)^2 - 2(x - x_o)\ddot{x}_o \\ &\quad -2(y - y_o)\ddot{y}_o \qquad (13) \\ D_2 &= -(\dot{y} - \dot{y}_o)v_x + (\dot{x} - \dot{x}_o)v_y \qquad (14) \end{aligned}$$

$\mathbf{M_o}$ being invertible when the first constraint is respected, we define the following change of coordinates:

$$\begin{bmatrix} u_1 \\ 2u_2 \end{bmatrix} := \mathbf{M_o}(\boldsymbol{\xi})\begin{bmatrix} F_{d,x} \\ F_{d,y} \end{bmatrix} \tag{15}$$

We then rewrite (12) as follows:

$$\begin{bmatrix} \ddot{d}_{o,2} \\ \dot{\phi}_\perp \end{bmatrix} = \begin{bmatrix} u_1 \\ u_2 \end{bmatrix} + \begin{bmatrix} D_1 \\ D_2 \end{bmatrix} \tag{16}$$

Let us now define $\dot{d}_{o,2} := \frac{d}{dt}d_{0,2} = 2d_o\dot{d}_o$ and the OIST tuning parameters $\kappa_2, \kappa_3, \kappa_4 > 0$.
We've got the following result:

Proposition 1 *Let us suppose that $d_{o,2}(t = 0) \geq d_{o,inf}^2$, $\dot{d}_{o,2}(t = 0) \geq -\kappa_1(d_{o,2}(t = 0) - d_{o,inf}^2)$ and $\phi_\perp(t = 0) \geq d_{o,inf}v_\perp^\# - \kappa_3(d_{o,2}(t = 0) - d_{o,inf}^2)$, then if for all $t \geq 0$,*

$$\begin{aligned} u_1 &\geq -(\kappa_1 + \kappa_2)\dot{d}_{o,2} - \kappa_1\kappa_2(d_{o,2} - d_{o,inf}^2) - D_1 \qquad (17) \\ u_2 &\geq -\kappa_3\dot{d}_{o,2} - \kappa_4(\phi_\perp - d_{o,inf}v_\perp^\# + \kappa_3(d_{o,2} - d_{o,inf}^2)) \\ &\quad -D_2 \qquad (18) \end{aligned}$$

then the output constraints (7)-(8) are satisfied for all $t \geq 0$.

proof: Straightforward applying Lemma 4.1 of [17].

Finally, it is required to express the input constraints in terms of the original control inputs.
It is easy to see that (17)-(18) are satisfied when one applies the following inputs:

$$\begin{bmatrix} F_{d,x}^{sat} \\ F_{d,y}^{sat} \end{bmatrix} = \mathbf{M_o}(\boldsymbol{\xi})^{-1} \begin{bmatrix} Sat^{+\infty}_{h_1(\dot{\xi},d_o,\dot{d}_0)}(u_1) \\ 2Sat^{+\infty}_{h_2(\dot{\xi},d_o,\dot{d}_0)}(u_2) \end{bmatrix} \tag{19}$$

where

$$\begin{aligned} h_1(\dot{\boldsymbol{\xi}}, d_o, \dot{d}_0) = &-D_1 - (\kappa_1 + \kappa_2)\dot{d}_{o,2} \\ &-\kappa_1\kappa_2(d_{o,2} - d_{o,inf}^2) \end{aligned} \tag{20}$$

$$\begin{aligned} h_2(\dot{\boldsymbol{\xi}}, d_o, \dot{d}_0) = &-D_2 - \kappa_3\dot{d}_{o,2} - \kappa_4(\phi_\perp - d_{o,inf}v_\perp^{\#}) \\ &-\kappa_3\kappa_4(d_{o,2} - d_{o,inf}^2)) \end{aligned} \tag{21}$$

Using (15), we finally obtain the following input saturations with time varying bounds :

$$\begin{bmatrix} F_{d,x}^{sat} \\ F_{d,y}^{sat} \end{bmatrix} \tag{22}$$

$$= \mathbf{M_o}(\boldsymbol{\xi})^{-1} \begin{bmatrix} Sat^{+\infty}_{h_1(\dot{\xi},d_o,\dot{d}_0)} \left(\begin{bmatrix} 1 \\ 0 \end{bmatrix}^T \mathbf{M_o}(\boldsymbol{\xi}) \begin{bmatrix} F_{d,x} \\ F_{d,y} \end{bmatrix} \right) \\ 2Sat^{+\infty}_{h_2(\dot{\xi},d_o,\dot{d}_0)} \left(\frac{1}{2} \begin{bmatrix} 0 \\ 1 \end{bmatrix}^T \mathbf{M_o}(\boldsymbol{\xi}) \begin{bmatrix} F_{d,x} \\ F_{d,y} \end{bmatrix} \right) \end{bmatrix} \tag{23}$$

4 SYSTEM ARCHITECTURE

4.1 Framework for experimentation

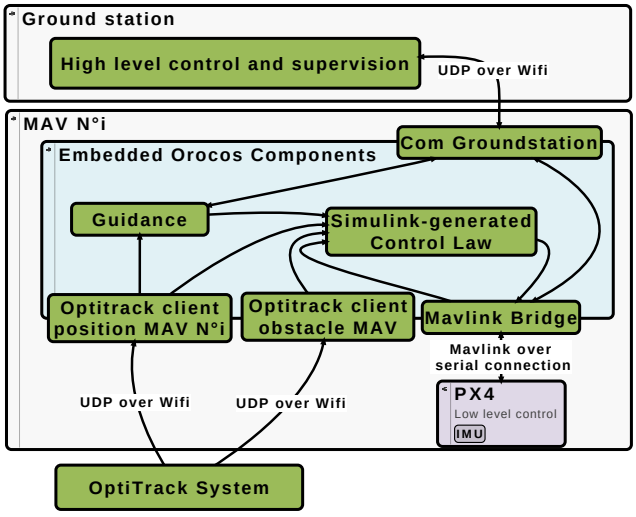

Figure 3: OIST formation framework

The framework that is used in our lab is described in [14] and allows many use cases, from the simple Simulink-only simulation to the experiments involving interaction between a real MAV and simulated sensors in the MORSE simulator. A variety of MAVs are available for experiments in our lab. For the formation flying experiment, the framework used (Fig. 3) was:

1. **Ground station:**

   A ground station was used to transmit high-level orders to the 3 MAVs using Wi-Fi. The high-level orders were "take off", "move formation to position $[x, y, z]$", "land", and "arm/disarm motors". It also monitored the battery level and position of the MAVs.

2. **Embedded Orocos components:**

   An Orocos component was used to relay the high-level orders received from the ground station to the guidance ("take off", "move to" and "land") and mavlink bridge ("arm/disarm motors") components. The MAV's desired position transmitted to the guidance component was offset to reflect the MAV N°i position in the formation. From the desired position, the guidance component was generating desired trajectories for positions and velocities without taking into account the obstacle. These trajectories were given to the Simulink-generated Orocos component which implemented the OIST control law. The OptiTrack was used to measure the MAV and MAV's obstacle positions at 50Hz.

3. **MAV N°$\mathbf{i}, \mathbf{i} \in \{0, 1, 2\}$:**

   The MAVs used were based on the mechanics of three Parrot AR.drone with custom electronics, a gumstix running the Orocos components and a Pixhawks PX4 for the attitude control.

4.2 Code-generation from Simulink models

Automatic code generation is used directly from Simulink to generate C++ Code which is included in the framework.

5 EXPERIMENT

In order to demonstrate the OIST obstacle avoidance methodology, we use it for the anti-collision of a fleet composed of three MAVs. The three MAVs take off on the ground at three different positions, then they go to their target point in the formation pattern. For i=0 to 2, each MAV N°i considers the MAV N°$i+1$ as a moving obstacle and will avoid it.(By convention MAV N°3 is MAV N°0 so that MAV N°2 avoids MAV N°0).

Figure 4 presents the trajectory of the MAVs with obstacle avoidance during the formation Establishment. A minimal distance of 80 centimeters has been chosen for the avoidance parameter.

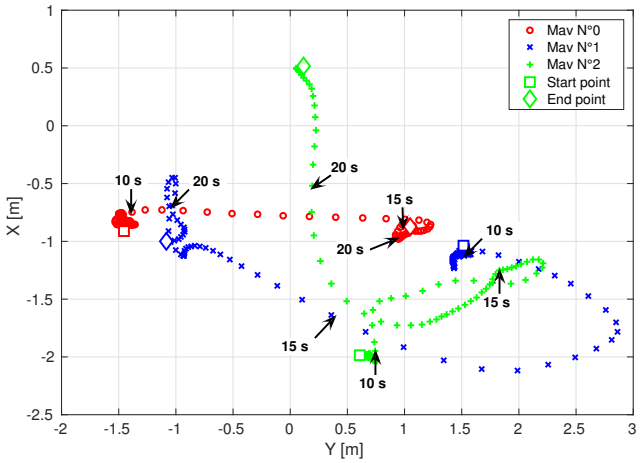

Figure 4: Trajectory of the 3 MAV's during the flight

One can see that the MAV N°0 is not deviated from the desired trajectory given by the guidance component. The two other MAVs are deviated by OIST as denoted on Fig. 5.

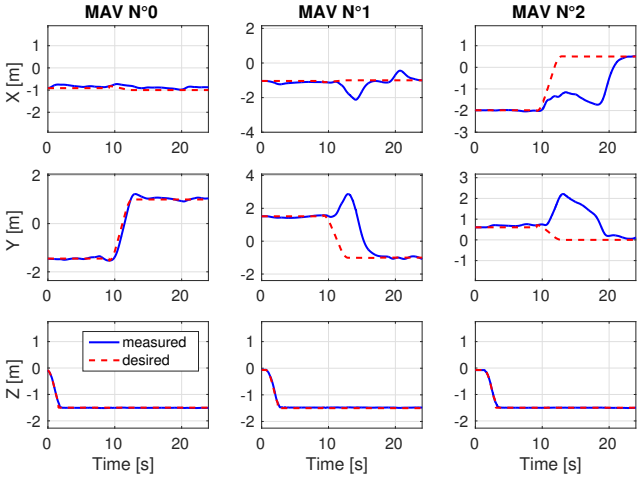

Figure 5: Positions of the 3 MAV's during the flight, the desired trajectories are computed without taking into account the obstacles

The avoidance results can be see on Fig. 6 which shows the saturation of the baseline thrust F_d by the OIST methodology, and the distance between the MAV N°i and its obstacle (the position of the MAV N°$i+1$).

For this experiment, the A.R.drone frame doesn't allow to increase the tracking performance of the position due to the lack of power. In our lab, the MAV based on Parrot weight more than 500 grams, which is 20 percent more than the nominal weight of the A.R.drone, so the thrust at the equilibrium point (for static flight) is about 75%. The dynamic cannot be very fast and we need to increase the minimal distance to 80 centimeters. On Fig. 6, the MAV N°2 is inside the avoidance

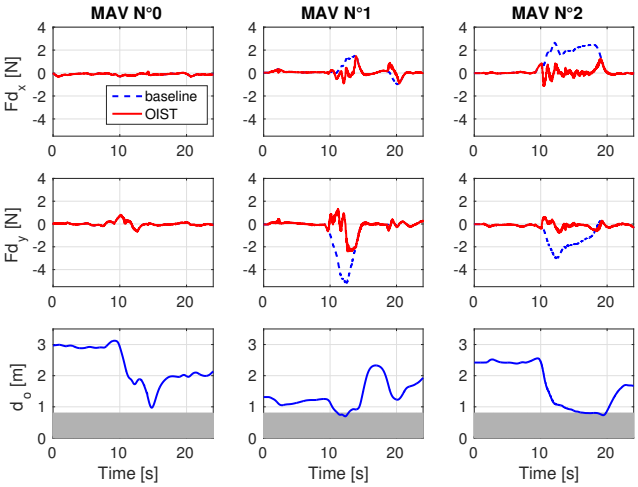

Figure 6: Saturation of the baseline thrust F_d and distance to obstacles during the flight

interval but as it is shown on Fig. 5, the tracking error is not minimal (about 20 centimeters of error) so this is more due to the position control.

In the video of this experiment [19], we can see that the MAVs avoid each other during the establishment of the formation. At the second 34 in the video (second 18 in the Figs. 4 to 6), we can see that even if the distance between the MAVs N°1 and N°2 is greater than 80 cm, the MAV N°1 still moves out of the way. This is because the OIST methodology also takes into account the velocity of the obstacle (MAV N°2 in this case). This effect can also be seen on the MAV N°2 between the seconds 10 to 12 when the MAV N°0 is approaching quickly.

6 CONCLUSIONS

In this paper, a novel framework to ensure anti-collision of a fleet of three MAVs has been presented. The OIST methology has been extended so that a MAV cannot be stuck on another MAV but turns around it. The main feature of this method is its simplicity in terms of control design and computational load. An experiment has been performed and validates the OIST methodology to ensure collision avoidance of up to three MAVs. The experimental results shows that the minimal distance between MAVs is globally respected during the establishment of the formation of the fleet. For the future experiments, MikroKopter-based MAVs will be used to increase the dynamics and the capabilities of the OIST methodology. Future works include rigourus stability proofs of saturated systems (in the spirit of [17]), extra experiments involving a larger number of MAVs and the extension of the OIST technique to address other problems related to safe guidance of multiple MAVs.

REFERENCES

[1] Y. Zhang and H. Mehrjerdi. A survey on multiple unmanned vehicles formation control and coordination: Normal and fault situations. In *2013 International Conference on Unmanned Aircraft Systems (ICUAS)*, pages 1087–1096, 2013.

[2] B. D. O. Anderson, B. Fidan, C. Yu, and D. Walle. *UAV Formation Control: Theory and Application*. Springer London, 2008.

[3] F. Giulietti, L. Pollini, and M. Innocenti. Autonomous formation flight. *IEEE Control Systems*, 20(6):34–44, 2000.

[4] Y. Watanabe, A. Amiez, and P. Chavent. Fully-autonomous coordinated flight of multiple uavs using decentralized virtual leader approach. In *2013 IEEE/RSJ International Conference on Intelligent Robots and Systems*, pages 5736–5741, 2013.

[5] L. V. Santana, A. S. Brando, and M. Sarcinelli-Filho. Heterogeneous leader-follower formation based on kinematic models. In *2016 International Conference on Unmanned Aircraft Systems (ICUAS)*, pages 342–346, 2016.

[6] R. W. Beard, T. W. McLain, D. B. Nelson, D. Kingston, and D. Johanson. Decentralized cooperative aerial surveillance using fixed-wing miniature uavs. *Proceedings of the IEEE*, 94(7):1306–1324, 2006.

[7] G. Gu, P. R. Chandler, C. J. Schumacher, A. Sparks, and M. Pachter. Optimal cooperative sensing using a team of uavs. *IEEE Transactions on Aerospace and Electronic Systems*, 42(4):1446–1458, 2006.

[8] A. Seuret, D. V. Dimarogonas, and K. H. Johansson. Consensus of double integrator multi-agents under communication delay. *FAC Proceedings Volumes*, 42(14):376 – 381, 2009. 8th IFAC Workshop on Time-Delay Systems.

[9] R. Olfati-Saber and R.M. Murray. Distributed cooperative control of multiple vehicle formations using structural potential functions. *FAC Proceedings Volumes*, 35(1):495 – 500, 2002. 15th IFAC World Congress.

[10] L. Garcia-Delgado, A. Dzul, V. Santibanez, and M. Llama. Quad-rotors formation based on potential functions with obstacle avoidance. *IET Control Theory Applications*, 6(12):1787–1802, 2012.

[11] A. Abdessameud and A. Tayebi. *Motion Coordination for VTOL Unmanned Aerial Vehicles*. Springer, 2013.

[12] L. Burlion. A new saturation function to convert an output constraint into an input constraint. In *Control Automation (MED), 2012 20th Mediterranean Conference on*, pages 1217–1222, 2012.

[13] L. Burlion and H. de Plinval. Keeping a ground point in the camera field of view of a landing uav. In *Robotics and Automation (ICRA), 2013 IEEE International Conference on*, pages 5763–5768, 2013.

[14] C. Chauffaut, F. Defay, L. Burlion, and H. de Plinval. Uav obstacle avoidance scheme using an output to input saturation transformation technique. In *2016 International Conference on Unmanned Aircraft Systems (ICUAS)*, pages 227–234, 2016.

[15] L. Burlion, C. Poussot-Vassal, P. Vuillemin, M. Leitner, and T. Kier. Longitudinal manoeuvre load control of a flexible large-scale aircraft. In *the 19th IFAC World Congress Conference*, pages 3413–3418, 2014.

[16] S. Galeani, S. Tarbouriech, M. Turner, and L. Zaccarian. A tutorial on modern anti-windup design. *European Journal of Control*, 15(34):418 – 440, 2009.

[17] E. Chambon, L. Burlion, and P. Apkarian. Time-response shaping using output to input saturation transformation. *International Journal of Control*, to appear in 2017.

[18] M. Lecointe, F. Defaÿ, and C. Carvalho Chanel. Backstepping control law application to path tracking with an indoor quadrotor. In *3rd CEAS EUROGNC Conf.*, 2015.

[19] C. Corentin, F. Defaÿ, L. Burlion, and H. de Plinval. Video of the oist experiment for collision avoidance in a fleet of three mavs, http://video.isae.fr/videos/?video=media170215164039955, 2017.